Influence of La incorporation on the catalytic activity of Ru/ETS-10 catalysts for hydrogen production

Betina Faroldi[1], Silvia Irusta[2], Laura Cornaglia,[1]*

[1] Instituto de Investigaciones en Catálisis y Petroquímica (FIQ, UNL-CONICET), Santiago del Estero 2829-3000 Santa Fe, Argentina

*E-mail: *lmcornag@fiq.unl.edu.ar*

Tel/Fax 54-342-4536861

[2] Instituto de Nanociencia de Aragón (INA), Universidad de Zaragoza, Mariano Esquillor s/n (50018), Zaragoza, España.

Abstract

The incorporation of lanthanum on ETS-10 titanosilicate and its influence on the catalytic activity of Ru catalysts for the dry reforming of methane reaction were studied. The catalysts were prepared through ion exchange of ETS-10 using different lanthanum solution concentrations (0.1, 0.2 and 0.4 % wt of La_2O_3). The Ru loading was 0.6 wt.% for all catalysts. The methane reaction rates for Ru/LaETS-10 catalysts showed an increase in comparison with Ru/ETS-10. This could be related to the lanthanum participation in the reaction mechanism. Moreover, all the formulations were stable after 70 h on stream.

In order to study the effect of lanthanum exchange in the structure of ETS-10 supports, the solids were characterized by BET, XRD, TEM, FTIR XPS, and Laser Raman spectroscopy.

The relative crystallinities were lower than 80%, indicating that the La exchange could have an important effect on the crystalline structure of ETS-10, in agreement with Raman and FTIR results.

The surface Ru/Ti ratio determined by XPS was higher in the case of Ru/LaETS-10 synthesized with the highest La concentration in the exchange solution. The Na/Ti ratio, measured by XPS and EDX, was lower for the Ru/LaETS-10 catalysts compared with ETS-10 suggesting that La was exchanged in the structure.

Keywords: Ru catalysts; ETS-10; Dry reforming of methane; hydrogen production

1. Introduction

The dry reforming of methane (DRM) is important from the environmental viewpoint since these two gases contribute to the green-house effect. The main advantage of the DRM reaction is that the H_2/CO ratio is low. This enables the use of syngas directly for the Fischer–Tropsch synthesis without further separation steps. When the goal of the methane reforming reactions is to produce hydrogen for use in a fuel cell, they can be carried out in membrane reactors that combine both the reaction and the hydrogen separation process in a single device [1,2].

One of the main challenges of this reaction is the preparation of an effective reforming catalyst without the deactivation produced by coke formation. In the presence of noble metals and an adequate support, coke formation can be attenuated. Dispersing the active metal on a high surface area solid and using the right promoters could improve the catalyst activity and stability.

Titanosilicate ETS-10 has some advantages over other similar materials, such as the possibility of synthesis based on different sources of Ti and the presence of a pure phase, which can be obtained in the absence of a structuring agent. Additionally, by functionalizing its structure, it is possible to modify its catalytic properties and adsorption isomorphic substitution, or its high ion exchange capacity, hydrophilicity and basicity [3,4,5].

Because of all these advantages and properties, ETS-10 has recently been used as catalyst support for various processes such as Ag/ETS-10 for aerobic oxidation of diphenyl [6], Cu/ETS-10 for NOx selective catalytic reduction [7], or Rh/ETS-10 for hydroaminomethylation [8], among other applications.

In a previous work, Shen and coworkers [9] reported that lanthanum-modified ETS-10 showed a good thermal and hydrothermal stability, for the n-hexadecane craking compared with the as-synthesized ETS-10 and the ammonium-exchanged ETS-10. Lanthanum hydroxyl groups can migrate to the ETS-10 channels or act as charge-balancing cations, which contributes to stabilize the framework of ETS-10.
Additionally, the lanthanum incorporation is an interesting alternative because it could participate as a reaction intermediate in the dry reforming reaction.
On the other hand, noble metals such as ruthenium, rhodium and platinum used as active phase show high resistance to coke deposition, which makes them suitable for the dry reforming reaction [10- 15]. However, the main drawback of using these active metal particles for catalysts is the high cost of the catalyst precursors. Given the low cost of ruthenium and its high activity compared with that of other noble metals, several studies employing Ru catalysts for the dry reforming of methane have recently been reported [10, 11]. The activity and selectivity of Ru catalysts greatly depend on the oxidation state [16] of the metal, which can change subject to both the reaction conditions and the support used [17].
The aim of this work is to study the incorporation of lanthanum on ETS-10 titanosilicate and its influence on the catalytic activity of Ru catalysts for the dry reforming of methane reaction at moderate temperatures (550 °C). The catalysts and supports were characterized using XRD, N_2 adsorption, ICP, SEM, TEM, EDX, FTIR, Raman spectroscopy and XPS to study the effect of lanthanum on the catalyst features.

2. Experimental

2.1. Preparation of catalysts and supports

The support was prepared according to the procedure used by Rocha et al [18]. To prepare a gel with composition 4.4 Na_2O/1.4 K_2O/TiO_2/5.5 SiO_2/125 H_2O, the following reactants were used: sodium silicate solution (25.5 to 28.5 % SiO_2, 7.5 to 8.5% Na_2O) (Merck), anatase 99.9% (Aldrich) as a source of Ti, NaCl (Carlo Erba), KCl (Riedel de Haen) and KF (Aldrich). The gel was introduced into an autoclave for 24 h at 230 ºC. Then the solid was filtered and washed until the washing water reached a pH between 9 and 10. Subsequently, the solid was dried at 100 º C in an oven for 12 h. La-exchanged titanosilicates were prepared from dried ETS-10 by conventional ion exchange with lanthanum nitrate solutions at room temperature.

Typically 1.25 g of solid sample were added to 100 ml of $La(NO)_3$ solution and the mixture was stirred at 80ºC for 24 h. After the exchange, the solids were centrifuged and washed until the pH was close to 7. The samples were dried at 90 ºC overnight and then calcined in flowing air at 550 ºC for 6 h. Different lanthanum solution concentrations (0.1, 0.2 and 0.4 % wt of La_2O_3) were used (nominal values). These values are indicated between parentheses La(X)-ETS-10.

$RuCl_3$ was added by incipient wetness impregnation on the La-ETS-10 supports and then dried at 90°C overnight. In all the catalysts, the Ru loading was 0.6% wt.

2.2. Catalyst characterization

Surface area. The BET surface area of the fresh solids was determined by N_2 adsorption at liquid nitrogen temperature using a Flowsorb 2300A apparatus from Micromeritics; the samples were degassed *in situ* during 8 h at 200ºC before carrying out the measurements.

X-ray diffraction (XRD). The XRD patterns of the uncalcined solids and supports were obtained with an XD-D1 Shimadzu instrument, using Cu Kα radiation at 30 kV and 40 mA. The scan rate was 1.0°/min for values between 2Θ = 5° and 45°.

Metal dispersion. The Ru dispersion of the fresh catalysts, following the in situ hydrogen reduction at 550 °C for 1 h, was determined by static equilibrium of H_2 adsorption at 100 ºC in a conventional vacuum system.

X-ray photoelectron spectroscopy (XPS). The XPS measurements were carried out using a multi-technique system (SPECS) equipped with a dual Mg/Al X-ray source and a hemispherical PHOIBOS 150 analyzer operating in the fixed analyzer transmission (FAT) mode. The spectra were obtained with pass energy of 30 eV; an Mg-Kα X-ray source was operated at 200 W and 12 kV. The working pressure in the analyzing chamber was less than 5.9 $x10^{-7}$ Pa. The XPS analyses were performed on the reduced solids after treatment with H_2 at 400 ºC carried out in the reaction chamber of the spectrometer. The spectral regions corresponding to O 1s, Si 2p, Si2s, Ti 2p, Na 1s, K 2p, C1s, Ru 3d and Ru 3p core levels were recorded for each sample. The photoelectron binding energies were referenced to the Si 2s peak, set at 153.7 eV.

The data treatment was performed with the Casa XPS program (Casa Software Ltd, UK). The peak areas were determined by integration employing a Shirley-type background. Peaks were considered to be a mixture of Gaussian and Lorentzian functions in a 70/30 ratio. The curve fitting was carried out taking into account the energy separation and the intensity ratio of each doublet pair for Ru 3d, Ru 3p and Ti 2p core levels. For the quantification of the elements, sensitivity factors provided by the manufacturer were used.

Laser Raman spectroscopy (LRS). The Raman spectra of fresh and used solids were recorded using a LabRam spectrometer (Horiba-Jobin-Yvon) coupled to an Olympus confocal microscope (a 100X objective lens was used for simultaneous illumination and collection), equipped with a CCD detector cooled to about 200 K using the Peltier

effect. The excitation wavelength was in all cases 532 nm (Spectra Physics diode pump solid state laser). The laser power was set at 30 mW.

Scanning electron microscopy (SEM). The morphology and particle sizes were studied with a SEM instrument (Hitachi S2300). In addition, samples were examined by SEM in a JEOL JSM-6400 instrument operating at 3-20 kV, which was used to perform the energy dispersive X-ray spectroscopy (EDX) analysis.

Transmission electron microscopy (TEM). TEM measurements were performed in a TEM 200: Tecnai T20, FEI and a HR Tecnai F30, FEI. Sample preparation was carried out by reducing a small portion (100 mg approx.) of fresh catalysts into a quartz reactor under a H_2 flow of 30 mL/min at 550ºC for 2 h. Once the catalyst was reduced, the reactor was cooled down to room temperature. A small amount of the reduced catalyst was ground in an agate mortar, suspended in a vial with approx. 4 mL of ethanol and stirred using an ultrasonic bath for a few minutes. Drops of this suspension were then added to a microscopy copper grid (Lacey Carbon Film coated copper grid 3.0 mm, 200 mesh, Pelco).

Fourier Transform Infrared Spectroscopy (FTIR). The FTIR spectra were obtained using a Shimadzu FTIR 8101 M spectrometer with a spectral resolution of 4 cm^{-1}. Fresh samples were crushed with pestle in an agate mortar. The crushed material was mixed with potassium bromide in a 1:100 proportion. The mixture was compressed by applying a pressure of 10 tons for 1 min. The FTIR spectra were recorded over the 4000– 400 cm^{-1} wavelength range.

2.3. Catalytic tests

The activity and stability for the dry reforming of methane of the Ru catalysts (2.5-20 mg diluted with 100 mg of quartz, particle size < 75 μm) were evaluated in a tubular

quartz reactor (inner diameter, 5 mm) which was placed into an electric oven. A thermocouple in a quartz sleeve was placed on top of the catalyst bed. The un-calcined catalysts were heated up to 550 °C in Ar flow and then reduced in H_2 flow at the same temperature for 2 h. After reduction, the reactant gas mixture (P_{CO2}:P_{CH4}:P_{Ar} = 1:1:1.2 , P = 100 kPa) was fed to the reactor. The reaction experiments were carried out at 550 °C.

The gas mixture composition was analyzed by gas chromatography with a thermal conductivity detector. More details were given in a previous work [17].

3. Results and discussion

3.1. Activity and stability tests in a conventional fixed-bed reactor

3.1.1. Effect of residence time on CH_4 reaction rates

Figure 1shows the CH_4 conversion measured at 550 ºC as a function of residence time on Ru/La(0.1)ETS-10. The residence time was expressed as W/F (catalyst mass/total flux). This experiment was performed with 15 mg of catalyst mass and varying the total flux between 90 and 187 cm^3 min^{-1}. The experimental values were aligned in a linear ratio between methane conversion and residence time. In this condition, it was observed that the measurements were not affected by transport effects. As a consequence, we can estimate the net methane reaction rates (r_n) from these experimental points. The reaction rates presented similar values in the range studied which was expected because the measurements were performed under differential conditions (Figure 1S in Supplementary data).

Additionally, in the same direction, the forward reaction rates (r_f) were calculated from the net rate of reaction in order to re-confirm the differential conditions. The r_f can be estimated as follows:

$$r_n = \frac{F_{AO}\ X_A}{W}$$

$$r_f = r_n(1-\eta)$$

$$\eta = \frac{(P_{CO})^2 (P_{H_2})^2}{P_{CH_4} P_{CO_2}} \frac{1}{Ke}$$

where F_{AO} is the feed molar flux of A species, X_A is the conversion of A species, W is the catalyst mass, P_i*s* are the prevalent pressures of reactants and products and *Ke* is the equilibrium constant calculated at the corresponding reaction temperature. The calculated η values were lower than 0.005, confirming the quality of the differential data obtained.

3.1.2. Comparison of the average reaction rates

The catalytic activity of the solids was evaluated in the DRM reaction in a conventional fixed bed reactor at 550 °C (Table 1). Ru/ETS-10, Ru/La_2O_3-SiO_2, Ru/La_2O_3, Ru/$La_2O_2CO_3$ and Ru ion exchanged into ETS-10 were included for comparison [1,3,17,19].

When lanthanum was exchanged in the ETS-10 titanosilicates, a significant increase in activity expressed as (mol CH_4 per gram of Ru per hour) was obtained for the Ru/La(X)ETS-10 catalysts in comparison with Ru/ETS-10 solid. The higher activities were obtained for the solids with the higher La content (0.2 and 0.4wt% of La_2O_3 in the exchanged solution).

In addition, these catalysts exhibited reaction rates higher than the Ru/La_2O_3-SiO_2 catalyst [19]. These high reaction rates could be related to the lanthanum participation in the reaction mechanism [17].

Furthermore, the metallic dispersion increased for Ru/La(X)ETS-10 catalysts with different lanthanum contents, reaching values between 42 to 65%. The turnover

frequency (TOF) was determined from the methane forward reaction rate (r_{CH4}) and the Ru dispersion (D_{Ru}) by the following expression:

$$TOF\left[\frac{1}{s}\right] = \frac{r_{CH_4}\left[mol\ CH_4/(mol\ Ru \cdot s)\right]}{D_{Ru}}$$

In a previous work [3], we reported that the forward CH_4 turnover frequencies increased with increasing Ru dispersion when ETS-10 was used as support, these results are summarized in the first lines of Table 1. This behavior was in agreement with what was reported by Wei and Iglesia [20, 21] for Ru, Rh and Pt supported on non-carbonate forming oxides such as Al_2O_3 or ZrO_2 for CH_4-CO_2 and CH_4-H_2O reactions.

The addition of lanthanum to the ETS-10 support modifies the behavior of the catalysts. In all cases, dispersions are higher than 42 %, nevertheless, TOF values do not follow the dispersion trend (Table 1). In fact, the catalyst with the higher dispersion (65%) has the lower TOF value.The increase of metal dispersion due to the presence of La was previously observed for Rh supported on SiO_2 [22], although for these catalysts the values of TOF did not follow the dispersion trend. The same happen for Ru/La_2O_3-SiO_2 solids, in which the metal-suport interaction would play an important role[19].

In the same way, Duarte et al. [23] reported the reaction rates of CH_4 per surface Rh atom of Rh/Al_2O_3 and Sm_2O_3-CeO_2 promoted catalysts for methane steam reforming (MSR) at 500 and 800ºC. The particle size was estimated from the first shell Rh–Rh coordination number determined from EXAFS analysis at high temperature under MSR conditions. Then, the reaction rates normalized per surface atom were calculated based on the dispersion determined under actual reaction conditions. The results obtained by these authors showed that the normalized reaction rates increased when the Rh particle size increased, in agreement with our observations for Ru catalysts.

The stability of the Ru/ETS-10 and Ru/La(X)ETS-10 was tested during 70 hours under reaction conditions (Figure 2). The methane conversion remained constant for all catalysts. The reaction rate of CO_2 (not shown) was always higher than the reaction rate of CH_4 due to the simultaneous occurrence of the reverse water gas shift reaction (RGWS). These values were consistent with the H_2/CO ratio lower than 1 observed for the three catalysts (Table 1). Furthermore, for all the used catalysts, no carbon deposition was detected through

Laser Raman spectroscopy, a technique that is highly sensitive to the presence of graphitic carbon.

3.2. Characterization of La(X)ETS-10 supports

The synthesized ETS-10 titanosilicate exhibited the typical morphology of the crystals in the form of truncated bipyramids with a particle sizes in the range of 400-500 nm (Figure 3) and a BET area equal to 266 m^2 g^{-1} with a pore volumen of 0.120 mL g^{-1}. Titanosilicate Ti atoms are octahedrally connected to four Si and two Ti atoms through oxygen bonds, giving rise to a three-dimensional structure with a significant degree of disorder [5]. The disordered material can be described by two ordered polymorphs, arranged in layers. The porous structure consisting of rings of 12, 7, 5 and 3 members has a three-dimensional pore system whose minimum diameter is defined by the 12-member rings, with a micropore size of 0.49 x 0.76 nm. A network of tetrahedral SiO_4 and octahedral TiO_6 is associated with a charge of -2 compensated by cations, mainly located in areas adjacent to the Ti chains and 12- and 7-member rings.

In order to study the effect of lanthanum exchange in the structure of ETS-10 supports the solids were characterized by BET, XRD, TEM, FTIR XPS, and Laser Raman spectroscopy.

After the exchange with lanthanum, the BET surface area was 219 m^2 g^{-1} for the La(0.4)ETS-10 support, similar to the value of the original ETS-10 [3]. However, the pore volumen decreased to 0.07 mL g^{-1}.

The Si/Ti ratios were measured by EDX for the La exchanged ETS-10 samples. As shown in Table 2, the values were similar for all solids. However, the Na/Ti ratio decreased from 2.2 to 0.4 when the La_2O_3 concentration of the exchange solution increased from 0.1 to 0.4 wt.%. Nevertheless, the K/Ti ratio slightly decreased. Tiscornia et al [24] and Ji et al [25] reported a preference to replace Na^+ ions in their Ag exchanged titanosilicates. The preferential exchange of Na^+ ions over K^+ ions was explained by the different locations of both cations. Na^+ ions are usually at the 12-membered ring pores whereas K^+ ions are located in the less accessible 7-membered rings.

The diffraction patterns of the La(X)ETS-10 samples prepared by ion-exchange using solutions with La_2O_3 concentrations of 0.1, 0.2 and 0.4 % wt are shown in Figure 4. The presence of ETS-10 [3] with a different degree of crystallinity was observed in all diffractograms.

The integration of the higher intensity peaks (2θ = 20, 24.5, 25.5, 35°) of each diffraction pattern was performed and the crystallinity was estimated. These results were compared with the data corresponding to the ETS-10 before the addition of lanthanum to calculate the loss of crystallinity (Table 3). The crystallinity was assumed to be 100% for the original ETS-10 sample. For the La(0.4)ETS-10 support, the crystallinity loss was equal to 75 %.

The stability of the ETS-10 structure were also studied by Laser Raman spectroscopy. Figure 5 shows the Raman spectra of the original ETS-10 and the La exchanged ETS-

10 samples. An important peak at ca. 730 cm^{-1} with a bandwidth (full width at half maximum, FWHM) of 35 cm^{-1}), together with other small peaks at 640, 514, 423, 396 band 305 cm^{-1}, and a high intensity peak at 144 cm^{-1} can be seen on the ETS-10-original sample. The low intensity peaks at 640, 514, and 396 cm^{-1} correspond to anatase TiO_2 modes, while, the high intensity band at 730 cm^{-1} was previously assigned to symmetric Ti–O stretching vibrations in octahedral TiO6 units along the –O–Ti–O–Ti–O– chains [26,27].

A significant reduction in the intensities of the Raman bands, mainly for the characteristic band at 730 cm^{-1}, can be found on the La exchanged ETS-10 samples. This peak was gradually broadened and shifted to a higher Raman shift (~800 cm^{-1} for La(0.4)ETS-10). Several authors [26,28] reported that both the position and the broadness of the band at about 725-730 cm^{-1} are indicative of the average length of the Ti–O–Ti–O– chain and the concentration of defects. Lv et al [26] observed that this band was considerably broadened and located at about 775 cm^{-1} in a highly defective ETS-10 material. The decrease in the intensity and disappearance of the peak at 724 cm^{-1} was ascribed to the partial or entire disruption of the –O–Ti–O–Ti–O–chains.

In our samples, the crystallinity and the modification in the intensity and position of the main Raman band could be ascribed to lanthanum exchange in the structure of ETS-10 titanosilicate.

3.2. Characterization of Ru/La(X)ETS-10 catalysts

For the Ru/La(X)ETS-10 catalysts, where Ru was incorporated by incipient wetness impregnation, similar XRD profiles were obtained. In Table 3, it can be observed that the crystallinity loss increases with the increase in the concentration of La_2O_3 in the

exchange solution. All the relative crystallinities are lower than 80%, indicating that the La exchange had an important effect on the crystalline structure of ETS-10.

Lv et al. [26] studied ETS-10 samples treated with nitric acid using solutions of different concentrations (pHs of 5–7). They reported that the acid-treated ETS-10 samples calcined at 550 °C showed a significant decrease in the diffraction intensities. They assigned this observation to the formation of an amount of terminal TiOH groups upon the acid treatment, which would condense at 550 °C, leading to structural dislocations and/or disorder. Note that in our samples the pH of the solutions was close to 5-6 after the ion-exchange with lanthanum nitrate.

The presence of lanthanum phases was also considered. The main reflection assigned to crystalline phases of lanthanum species (La_2O_3, $La(OH)_3$ and $La_2O_2CO_3$) could overlap with the reflection at 27 ° from the ETS-10 phase. The ratios of the peaks at 2θ = 24.5 and 27 ° ($I_{24.5}/I_{27}$) and at 2θ = 24.5 and 20 ° ($I_{24.5}/I_{20}$) were calculated for all samples. These values were compared with those of the titanosilicate before the incorporation of lanthanum. The $I_{24.5}/I_{20}$ intensity ratio, that corresponds to both ETS-10 reflections, did not change after lanthanum exchange. However, the $I_{24.5}/I_{27}$ ratio was 5.1 for the ETS-10 sample and decreased after the La incorporation. For the sample with higher La content, the ratio was 2.9, which may indicate some contribution (presence of) from lanthanum crystalline phases.

Figure 6 shows the Raman spectra of the Ru catalysts. The characteristic ETS-10 Raman band at 730 cm^{-1} significantly reduced its intensity as observed for the La exchanged support. No peaks assigned to lanthanum phases such us oxycarbonate (peak at 1080 cm^{-1}) were observed.

For the same purpose, FTIR spectra of the Ru prepared solids are also presented in Figure 7. The broad absorption bands at 1200-900 cm-1 were previously assigned to

the overlap of the stretching vibrations due to Si-O-Si, Si-O-Ti, and Si-O-. In our ETS-10 spectrum, the vibrations are found at 1160, 1032, 990 (shoulder); in addition, bands at 739, 637(low) and 550 cm^{-1} are observed. The band at 739 cm^{-1} decreases its intensity with increasing La exchange, in agreement with Raman results.

Tiscornia et al. [24] linked the decrease in the band at 885 cm^{-1}, observed after Ag exchange, to the perturbations of the T-O-T framework bonds induced by cations in zeolites with relatively low-aluminum content (Si/Al > 6) and found in the 920-880 cm^{-1} region.

Transmission electron microscopy images allow visualizing the single crystal nature of individual ETS-10, even of nanometer size crystals [29,30]. In the La(0.4) ETS-10 particle, the well-defined pattern of ETS-10 is clearly seen (Fig. 8.a). X-ray energy dispersive spectroscopy analysis confirmed that the observed particles contained lanthanum. In the case of the Ru/La(0.4)ETS-10 catalyst, a particle with its c axis oriented perpendicularly to the plane of the picture (c plane) can be seen and the presence of Ru nanoparticles with sizes between 3-5 nm distributed over the support (Fig. 8.b) is also evident.

An XPS analysis was performed in order to obtain information on surface structure and composition of the Ru/La(X)ETS-10 solids. The XPS measurements were performed on samples reduced at 400°C in a H_2/Ar mixture carried out in an atmospheric pressure reactor attached to the spectrometer. An overlap between Ru 3d and the carbonaceous contamination C 1s peak at 284.6 eV was observed. The C1s spectra also exhibited a very low intensity peak at 287.8 eV that was attributed to carbonaceous species associated with oxygen and/or hydrogen. After reduction, the Ru $3d_{5/2}$ peak always appeared at 280 ± 0.2 eV that corresponds to Ru^0. In addition,

the Ti 2p - Ru $3p_{3/2}$ region was analyzed due to the overlapping of C 1s and Ru 3d contributions. Figure 9.a shows the Ru $3p_{3/2}$ spectra for the ETS-10 and the reduced catalysts. A shift to 460.4 eV in the reduced solid with respect to that at 463.8 eV peak assigned to Ru^{+n} species [31] was observed. This change confirms the surface reduction to Ru^0 upon treatment with hydrogen.

A Ti $2p_{3/2}$ peak positioned at 458.9 eV can also be observed, which is due to the octahedral Ti atoms in the –O–Ti–O–Ti–O– chains of ETS-10. This signal does not change its BE in the exchanged samples, in agreement with several authors [32] that observed no significant changes with Li^+, Na^+, K^+, Rb^+, Cs^+ and Ba^+ as exchanged cations. However, an increase in the Ti $2p_{3/2}$ binding energies with the addition of Al, Bi and Fe in mesoporous titanosilicates was reported [32]. In addition, no peaks related to Ti(III) species (BE= 457 eV) or peaks associated with tetrahedral Ti species (BE=459.1 eV) were detected. The latter was also attributed to the five-coordinated titanium atoms appearing in the defects of –O–Ti–O–Ti–O– chains or on the external surfaces, where –O–Ti–O–Ti–O– chains end, in the case of acid treated ETS-10 samples.

Fig. 9.b shows the O 1s core level XPS spectra of ETS-10 titanosilicate. The peak can be fitted in two contributions, the high intensity peak 531.9 eV attributed to oxygen atoms in the Si-O-Si and Si-O-Ti linkages, and the lower intensity peak at 530.2 eV, due to oxygen atoms in Ti-O-Ti linkages. The fitted data are presented in Table 4.

For the Ru/La(X)ETS-10 catalysts, the same contributions were observed. However, the relative intensity of the peak due to oxygen atoms in the Ti–O–Ti linkage was gradually increased with increasing La content. Compared to the ETS-10 sample, the

relative area ratio of the peak at about 530.1 eV in Ru/La(0.4) ETS-10 was increased from 24% to 60 %.

For the lanthanum species (Table 4), the binding energies and the main peak – satellite splits were close to 3.7 eV and the main peak to satellite (shake up) peak intensity ratio was approximately 0.93 ± 0.2 eV, slightly higher than the value observed in the lanthanum oxide (0.77), in agreement with those previously reported for La exchanged zeolites [33] and Ru/La_2O_3-SiO_2 catalysts [19]. In these previous studies, [33,34] the authors compared the La signal shapes of La_2O_3 and of La zeolites, and attributed the decreased contribution of the high-BE La component in the zeolites to the fact that the La ions are coordinated by H_2O molecules and by oxygen engaged in the partially covalent bonding of the zeolite framework. In the Ru/ La_2O_3-SiO_2 catalysts, the difference was assigned to the possible formation of a well-dispersed lanthanum disilicate phase on the support surface. In the case of La(X)ETS-10 catalyts, the high value of the main peak to satellite (shake up) peak intensity ratio (0.77 for La_2O_3) could be related to the presence of LaOx exchanged species. In addition, the surface atomic concentration of La also increased when the La_2O_3 content in the exchange solution increased.

In the case of the acid treated sample reported by Lv et al [26], they observed a decrease in the intensity of the 530.1 eV peak. They assigned this decrease to the formation of the Ti vacancy resulting from the partial leaching of Ti atoms under acidic conditions, and to the interruption of –O–Ti–O–Ti–O– chains, which can lead to the change in the coordination state of Ti atoms.

The elemental composition of the catalysts and the ETS-10 was studied by XPS and the results are summarized in Table 4. The Na/Ti ratio for the support and Ru/ETS-10 was

similar, whereas this value decreased for the case of samples exchanged with lanthanum. This could suggest that the La was exchanged in the structure of ETS-10. However, in these solids the K/Ti ratio remained constant. Thus, in these Ru/La-ETS samples La^{3+} ions gradually replaced Na^{+} ions in agreement with the EDX results (Tabla 2). The surface metal concentration (Ru/Ti) was higher in the case of Ru/La(0.4)ETS-10. Bianchi and Ragaini [32] considered the atomic M/Ti ratio as a measure of the penetration of metal M in the interior of the pores of ETS-10, modified by ion exchange with ions of alkali metals. They observed that this ratio increases when the radius of the alkali metal exchanged increases. The M/Ti ratio is very high when the active metal cannot penetrate the pores, due to steric constraints of the exchanged cations. In our catalysts with higher content of lanthanum, this element can partially occupy the pores producing a steric restriction for Ru nanoparticles.

4. Conclusions

The incorporation of lanthanum on ETS-10 titanosilicate significantly improved the catalytic activity of Ru catalysts for the dry reforming of methane reaction.

The results of the characterization techniques suggest that lanthanum could be exchanged in the structure of the ETS-10. The crystallinity loss and the modification in the intensity and position of the main Raman band could be ascribed to lanthanum exchange in the structure of ETS-10 titanosilicate. In addition, TEM images and EDX analysis allow visualizing particles contained lanthanum and Ru nanoparticles with sizes between 3-5 nm distributed over the support.

In order to obtain information on the surface structure, a XPS analysis was performed on

the reduced catalyts. The relative intensity of the O1s peak due to oxygen atoms in the Ti–O–Ti linkage gradually increased with increasing La content. Furthermore, the analysis of the main peak and shake up satellite features for the La 3d core level indicated the presence of LaOx exchanged species.

Ru catalysts based on La modified-ETS-10 titanosilicates were active and also very stable for this reaction. For these La based supports, the results showed that the turnover frequencies increased when the Ru particle size increased, in agreement with our previous observations for Ru and Rh catalysts supported on different lanthanum based-systems. This behaviour could be related to the lanthanum participation in the reaction mechanism.

Acknowledgments

The authors wish to acknowledge the financial support received from ANPCYT, UNL and CONICET. Thanks are also given to ANPCyT for Grant PME 8 – 2003 to finance the purchase of the UHV Multi Analysis System, to the Japan International Cooperation Agency (JICA) for the donation of the major instruments used in this study, and to Prof. Elsa Grimaldi for the English language editing.

References

[1] B. Faroldi, C. Carrara, E.A. Lombardo, L. Cornaglia, Appl. Catal. A: Gen. 319 (2007) 38-46.

[2] B. Faroldi, E. Lombardo, L. Cornaglia, Catal. Today 172 (2011) 209– 217.

[3] B. Faroldi, E. Lombardo, L. Cornaglia, S. Irusta, Appl. Catal. A: Gen. 417– 418 (2012) 43–52.

[4] J. Rocha, M. Anderson, Eur. J. Inorg. Chem. 5 (2000) 801-818.

[5] M. Anderson, O. Terasaki, T. Oshuna, P. Malley, A. Philippou, S. MacKay, A. Ferreira, J. Rocha, S. Lidin, Philos. Mag. B 71 (1995) 813-841.

[6] S. Galioglu, M. Zahmakiran, Y. Kalay, S. Ozkar, B. Akata, Micropor. Mesopor. Mater. 159 (2012) 1-8.

[7] L. Song, Z. Zhan, X. Liu, H. He, W. Qiu, X. Zi, Ch J Catal 35 (2014) 1030-1035.

[8] N. Sudheesh, R. Shukla, Appl. Catal. A: Gen. 473 (2014) 116-124.

[9] H. Li, B. Shen, X. Wang and S. Shen, Catal Letters 99 (2005) 165-169.

[10] D. Carvalho, H. de Souza, J. Filhob, A.Oliveira, A. Campos, É. Milet, F. de Sousa, E. Padron-Hernandez, A. Oliveira, Appl. Catal. A: Gen. 473 (2014) 132–145.

[11] A. Derk, G. Moore, S. Sharma, E. McFarland, H. Metiu, Top. Catal. 57 (2014) 118–124.

[12] Zs. Ferencz, K. Baán, A. Oszkó, Z. Kónya, T. Kecskés, A. Erdóhelyi, Catal Today 228 (2014) 123-130.

[13] D. Pakhare and J. Spivey, Chem. Soc. Rev., 43 (2014) 7813-7837.

[14] N.Mota, C. Alvarez-Galvan, R.M. Navarro, J.L.G. Fierro, Biofuels, 2 (2011) 325-343.

[15] M.-S. Fan, A.Z. Abdullah, S. Bhatia, Chem Cat Chem 1 (2009) 192-208.

[16]K. Nakagawa, S. Hideshima, N. Akamatsu, N. Matsui, N. Ikenaga, T. Suzuki, CO_2 Conversion and Utilization, Chap. 14. ACS symposium series. ACS, Washington DC, (2002) 205–233.

[17] B. Faroldi, J. Múnera, L. Cornaglia, Appl. Catal. B: Environmental 150– 151 (2014) 126–137.

[18] J. Rocha, A. Ferreira, Z. Lin, M. Anderson, Micropor. Mesopor. Mater. 23 (1998) 253-263.

[19] B.M. Faroldi, E. Lombardo, L. Cornaglia, Appl. Catal. A: Gen. 369 (2009) 15–26.

[20] J.M. Wei, E. Iglesia, J. Phys. Chem. B. 108 (2004) 4094-4103.

[21] J.M. Wei, E. Iglesia, J. Phys. Chem. B. 108 (2004) 7253-7262.

[22] S. Irusta, J. Múnera, C. Carrara, E. Lombardo, L.Cornaglia, Appl. Catal. A: Gen. 287 (2005) 147–158.

[23] R. Duarte, M. Nachtegaal, J.M.C. Bueno, J.A. van Bokhoven, J. Catal. 296 (2012) 86-98.

[24] I. Tiscornia, S. Irusta, P. Prádanos, C. Téllez, J. Coronas, J. Santamaría, J. Phys. Chem. C 111 (2007) 4702-4709.

[25] Z. Ji, M. Ismail, D. Callahan Jr., E. Pandowo, Z. Cai, T. Goodrich, K. Ziemer, J. Warzywoda, A. Sacco Jr., Appl. Catal. B: Environmental 102 (2011) 323–333.

[26] L. Lv, F.Y. Lee, J. Zhou, F. Su, X.S. Zhao, Micropor. Mesopor. Mater. 96 (2006) 270–275.

[27] N. Jeong, Y. Lee, K. Byung Yoon, Micropor. Mesopor. Mater. 115 (2008) 308–313.

[28] P.D. Southon, R.F. Howe, Chem. Mater. 14 (2002) 4209-4218.

[29] X. Yang, J. Paillaud, H. van Breukelen, H. Kessler, E. Duprey, Micropor. Mesopor. Mater. 46 (2001) 1-11.

[30] F.X.L.I. Xamena, P. Calza, C. Lamberti, C. Prestipino, A. Damin, S. Bordiga, E. Pelizzetti, A. Zecchina, J. Am. Chem. Soc. 125 (2003) 2264–2271.

[31] C. Carrara, J. Múnera, E. Lombardo, L. Cornaglia, Top. Catal. 51 (2008) 98–106.

[32] G. Yan, T. Wu, W. Weng, H. Toghiani, R.K. Toghiani, H.L.Wan, C.U. Pittman, J. Catal. 226 (2004) 247-259.

[33] L.Gutierrez and E. Lombardo, Appl. Catal. A: General 360 (2009) 107‑119.

[34] W. Grünert, U. Sauerlandt, R. Schlögl, H.G. Karge, J. Phys. Chem. 97 (1993) 1413-1419.

[35] C.L. Bianchi, V. Ragaini, J. Catal. 168 (1997) 70–74.

Table 1. Support BET surface area, metal dispersion (D_{Ru}) and catalytic activity of Ru catalysts for the dry reforming of CH_4 at 550 ºC.

Catalysts	r_{CH4} [mol/g Ru h]	D_{Ru} [%]	TOF [s^{-1}]	H_2/CO	BET surface area [m^2 g^{-1}]	Ref.
Ru/ETS-10 [a]	40.0	9	12.5	0.29	266	[3]
Ru-exchanged/ETS-10[b]	6.0	5	3.4	0.35	266	[3]
Ru/La(0.1)ETS-10 [a,c]	78.3	65	3.4	0.45	279	This work
Ru/La(0.2)ETS-10 [a,c]	100.0	42	6.7	0.31	-	This work
Ru/La(0.4)ETS-10 [a,c]	96.7	47	5.8	0.35	219	This work
Ru/La_2O_3(15)-SiO_2 [a,d]	56.7	36	4.4	0.27	188	[19]
Ru/La_2O_3(27)-SiO_2 [a,d]	35.0	24	4.1	0.26	143	[19]
Ru/La_2O_3(40)-SiO_2 [a,d]	30.0	29	2.9	0.37	88	[19]
Ru/La_2O_3(50)-SiO_2 [a,d]	66.7	36	5.2	0.36	53	[19]
Ru/$La_2O_2CO_3$ [e]	38.3	19	5.6	0.30	31	[17]
Ru/La_2O_3 [e]	35.0	5	19.7	0.30	5	[1]

[a]Ru (0.6wt%) was incorporated by incipient wetness impregnation over ETS-10 or La(X)ETS-10 or La_2O_3-SiO_2.

[b]Ru (1wt%) was incorporated by ion exchanged into ETS-10.

[c]The wt.% of La_2O_3 in exchanged solution is indicated between parentheses.

[d]The wt.% of La_2O_3 is indicated between parentheses.

[e]Ru (0.6 wt%) was incorporated by wet impregnation over La_2O_3 or $La_2O_2CO_3$.

Table 2. Atomic ratios of elements measured by EDX for the supports.

Solids	Si/Ti	La/Ti	Na/Ti	K/Ti	(La+K+Na)/Ti
ETS-10	4.5	-	2.2	0.4	2.6
La(0.1)ETS-10	4.2	0.3	1.0	0.3	1.6
La(0.2)ETS-10	4.4	0.6	0.5	0.3	1.5
La(0.4)ETS-10	4.0	0.5	0.4	0.2	1.1

Table 3. Analysis of XRD patterns of Ru/catalysts compared with ETS-10 and La(0.4)ETS-10.

Solids	$I_{24.5}/I_{27}$ [a]	$I_{24.5}/I_{20}$ [b]	Crystallinity (%)	Crystallinity loss (%)
ETS-10	5.1	3.9	100	0
La(0.4)ETS-10	3.1	4.1	25	75
Ru/La(0.1)ETS-10	4.7	4.1	77	23
Ru/La(0.2)ETS-10	4.5	4.0	48	52
Ru/La(0.4)ETS-10	2.9	4.2	23	77

[a]Intensity ratios of reflections at 2θ= 24.5 and 27º.

[b]Intensity ratios of reflections at 2θ= 24.5 and 20º.

Table 4. XPS binding energies (eV) for O 1s and La 3d core levels, and surface atomic intensity ratios for ETS-10 and Ru catalysts reduced at 400ºC.

Samples	O 1s[b]	La $3d_{5/2}$[c]	Isat / IMP)[d]	ΔMP Sat[e]	La/Ti	Na/Ti	K/Ti	Si/Ti	Ru 3p/Ti	Ru 3d/Ti
ETS-10	530.4 (24) 532.1 (76)	-	-	-	-	1.20	0.6	6.3	-	-
Ru/ETS-10[a]	530.5 (30) 532.2 (70)	-	-	-	-	1.60	0.7	5.9	-	0.28
Ru/La(0.1)ETS-10[a]	530.4 (35) 532.1 (65)	835.0 (2.8)	0.96	3.6	0.80	0.70	0.7	6.2	0.49	0.43
Ru/La(0.2)ETS-10[a]	530.7 (58) 532.4 (42)	835.2 (2.8)	0.93	3.5	0.97	0.53	0.5	7.1	0.61	0.76
Ru/La(0.4)ETS-10[a]	530.7 (60) 532.5 (40)	835.1 (3.0)	0.92	3.5	2.20	-	0.6	8.9	0.71	0.84

[a]Ru (0.6 wt. %) was incorporated by incipient wetness impregnation over ETS-10 or La(X)ETS-10.

[b]Relative intensity ratio of each O 1s peak is shown between parenthesis.

[c] FWHM (eV) are shown between parenthesis. [d]Satellite / main peak intensity ratio for La $3d_{5/2}$. [e]Main peak - satellite splits for La $3d_{5/2}$.

For all samples, the binding energy of Si 2s peak was set at 153.7 eV.

Figure Legends

Figure 1.a. CH_4 conversion as a function of residence time (W/F) for Ru/La(0.1)ETS-10 varying total flux between 90 and 187 cm^3 min^{-1} (Reaction temperature = 550ºC, P= 100 kPa, feed composition: P_{CH4}:P_{CO2}:P_{Ar} = 1:1:1.1).

Figure 2. Stability test of the catalysts after reduction at 550ºC in the fixed-bed reactor (Reaction temperature = 550ºC, P= 100 kPa, W/F=4.3 x 10^{-6} g h cm^{-3} (; feed composition: P_{CH4}:P_{CO2}:P_{Ar} = 1:1:1.1).

Figure 3. SEM imagen of crystalline materials of ETS-10 with a synthesis time of 24 h at 230ºC.

Figure 4. XRD patterns of La(X)ETS-10 supports with different lanthanum contents.

Figure 5. Laser Raman spectra of La(X)ETS-10 supports compared with ETS-10.

Figure 6. Laser Raman spectra of Ru/La(X)ETS-10 fresh catalysts.

Figure 7. FTIR spectra of Ru/La(X)ETS-10 and Ru/ETS-10 catalysts.

Figure 8. TEM images of La(0.4)ETS-10 support (a) and reduced Ru/La(0.4)ETS-10 catalyst (b).

Figure 9. XPS spectra of Ti 2p – Ru 3p (a) and O 1s (b) regions for Ru/catalysts compared with ETS-10.

Suplementary Files

Figure 1S. Net CH_4 reaction rate as a function of residence time for Ru/La(0.1)ETS-10 (Reaction temperature = 550ºC, P= 100 kPa, feed composition: P_{CH4}:P_{CO2}:P_{Ar} = 1:1:1.1).

Figure 1.

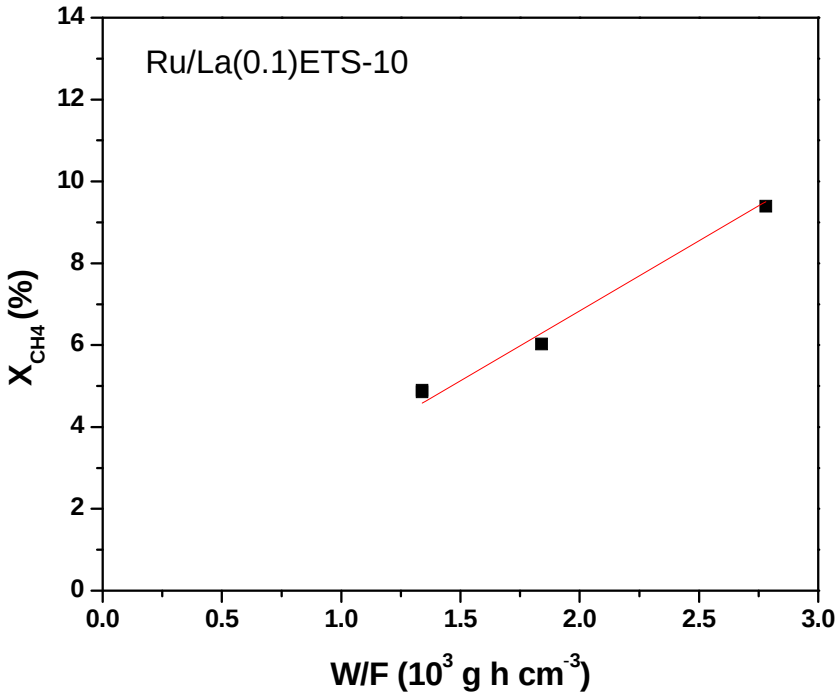

Figure 2.

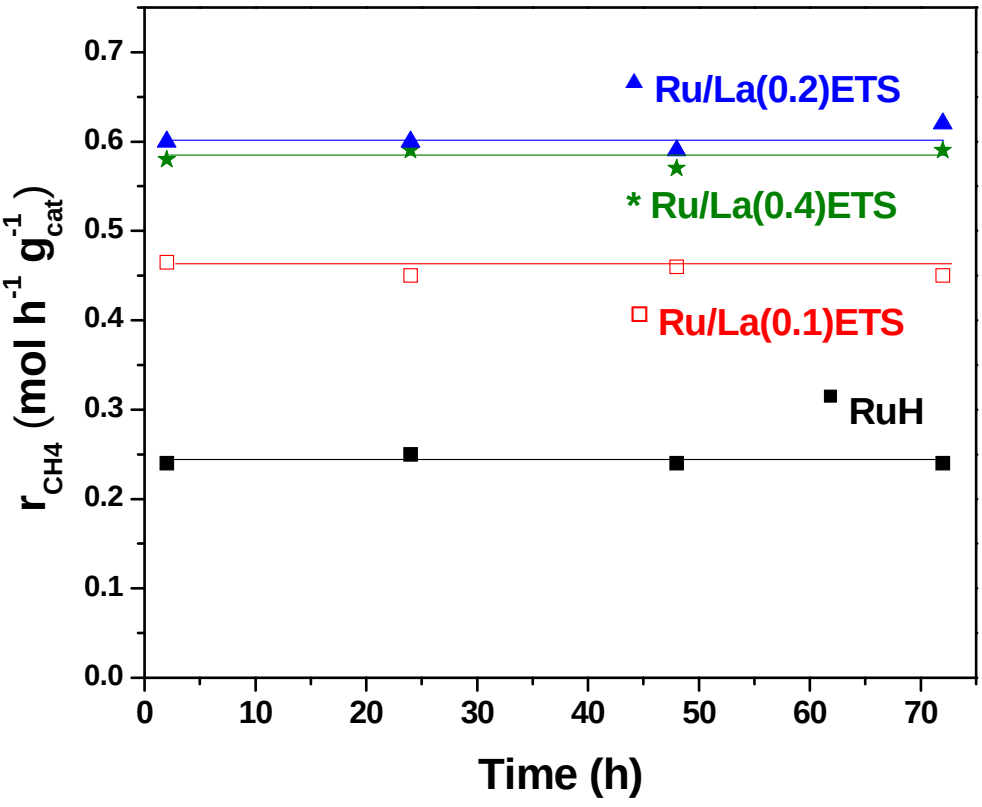

Figure 3.

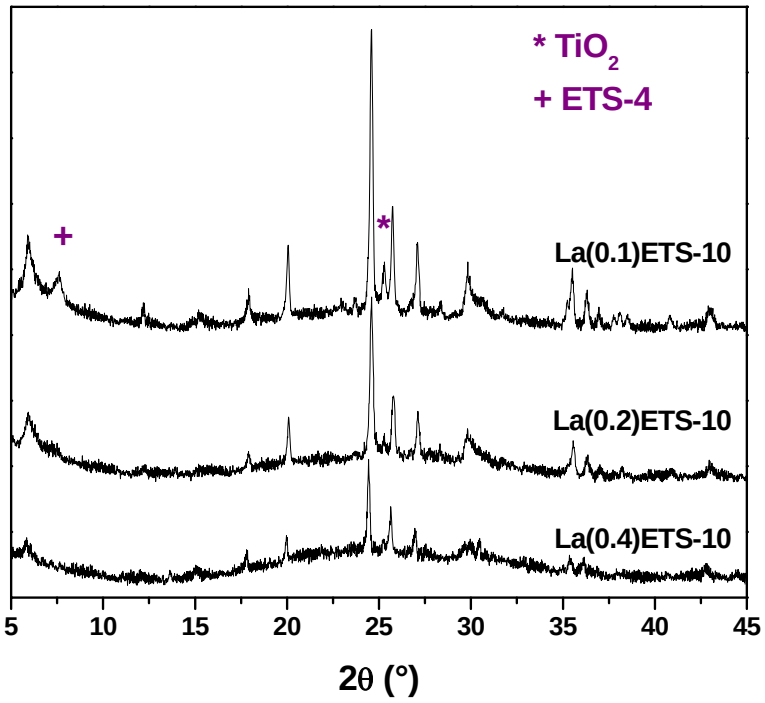

Figure 4

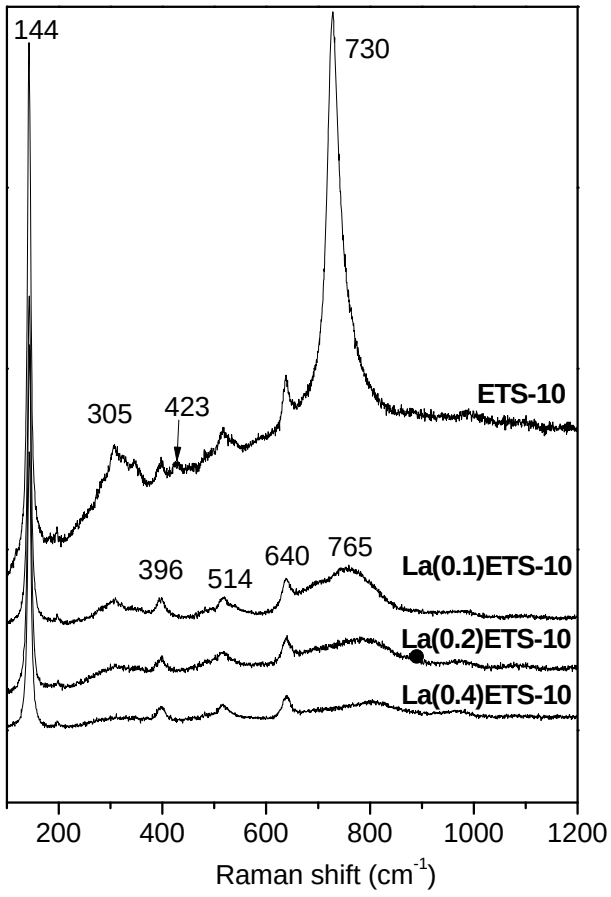

Figure 5

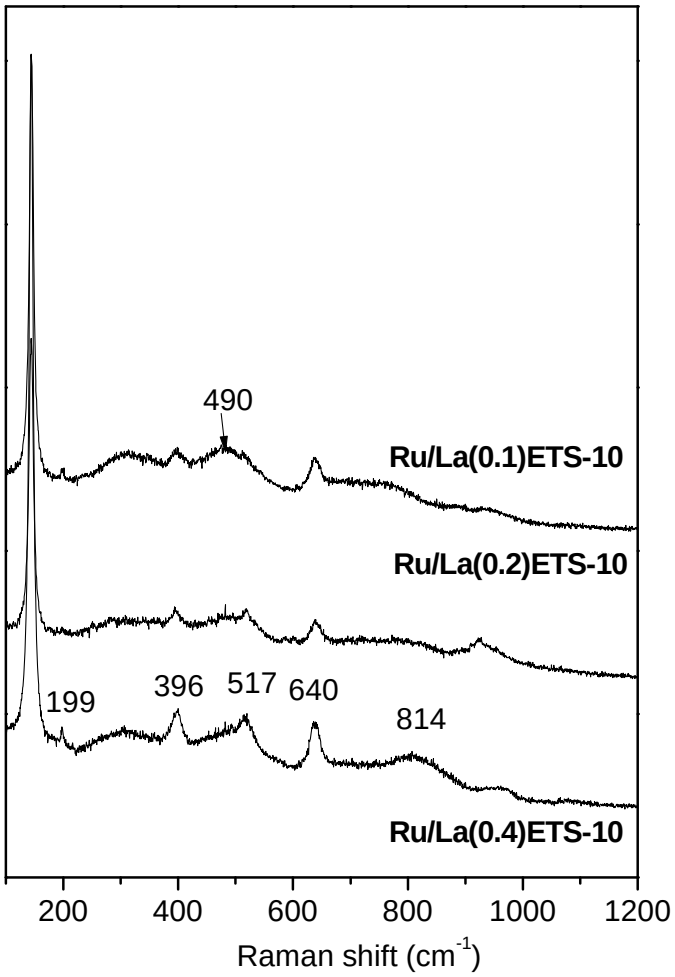

Figure 6

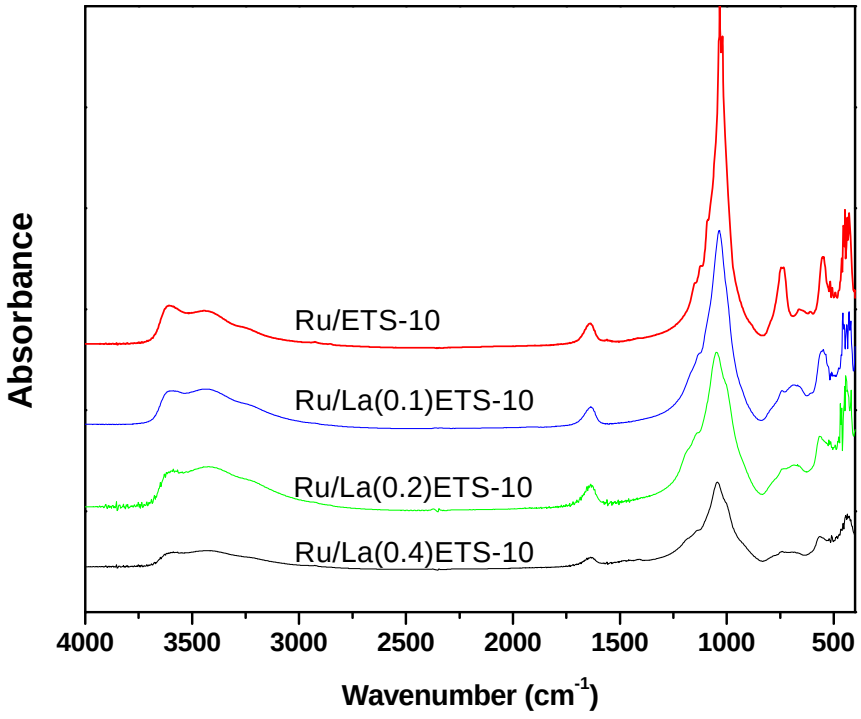

Figure 7

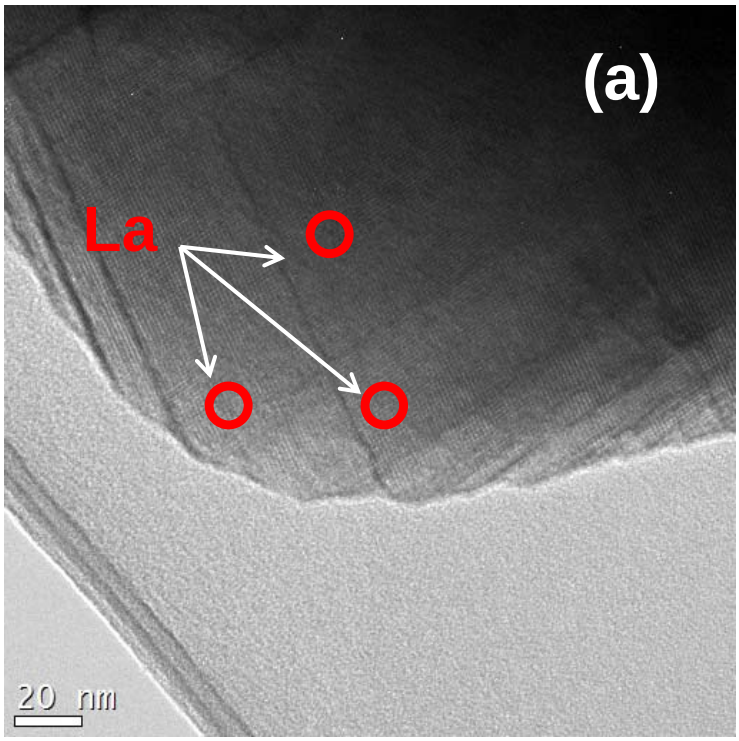

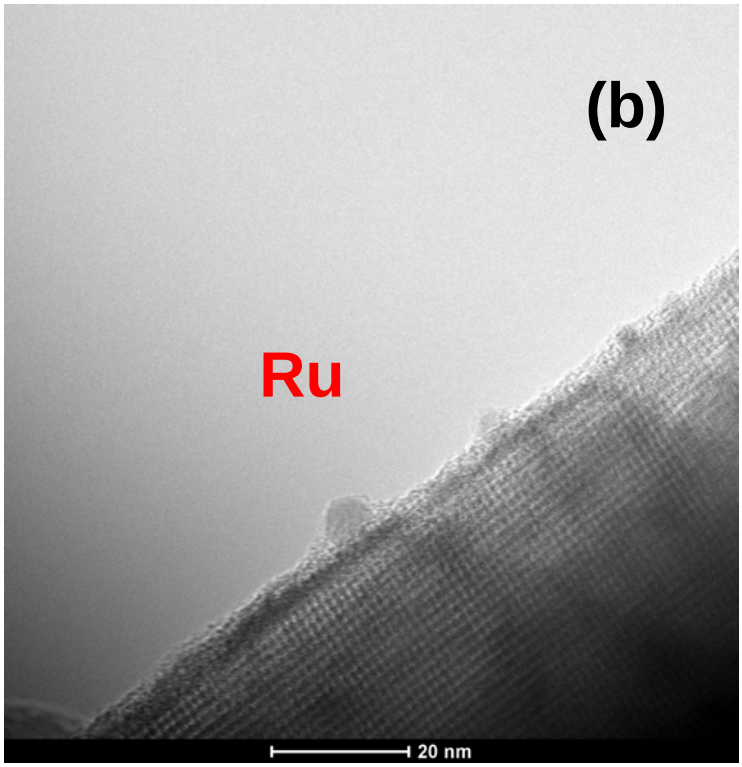

Figure 8.

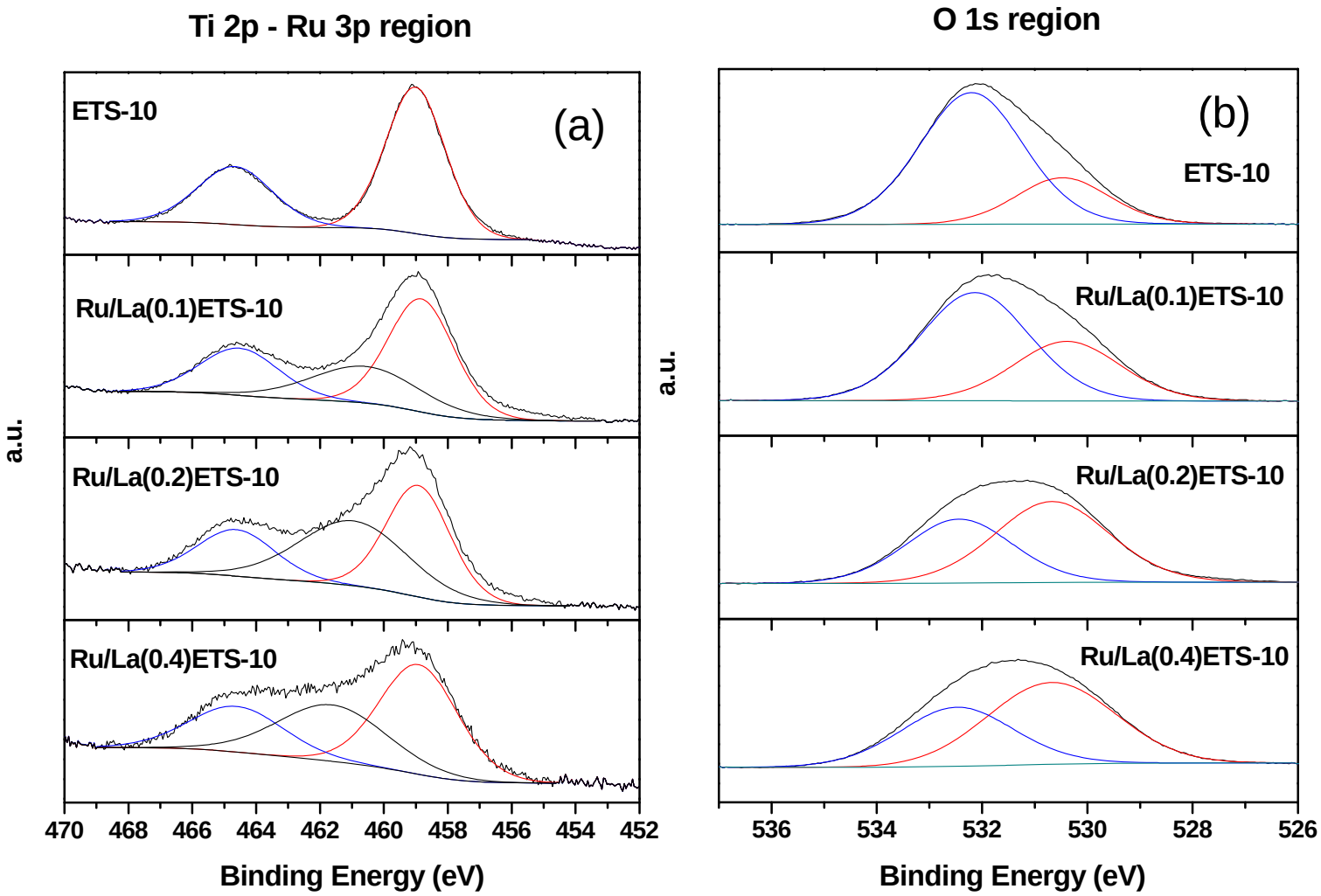
Ti 2p - Ru 3p region
O 1s region
ETS-10
(a)
Ru/La(0.1)ETS-10
Ru/La(0.2)ETS-10
Ru/La(0.4)ETS-10
a.u.
470
468
466
464
462
460
458
456
454
452
Binding Energy (eV)
(b)
ETS-10
Ru/La(0.1)ETS-10
Ru/La(0.2)ETS-10
Ru/La(0.4)ETS-10
a.u.
536
534
532
530
528
526
Binding Energy (eV)

Figure 1S

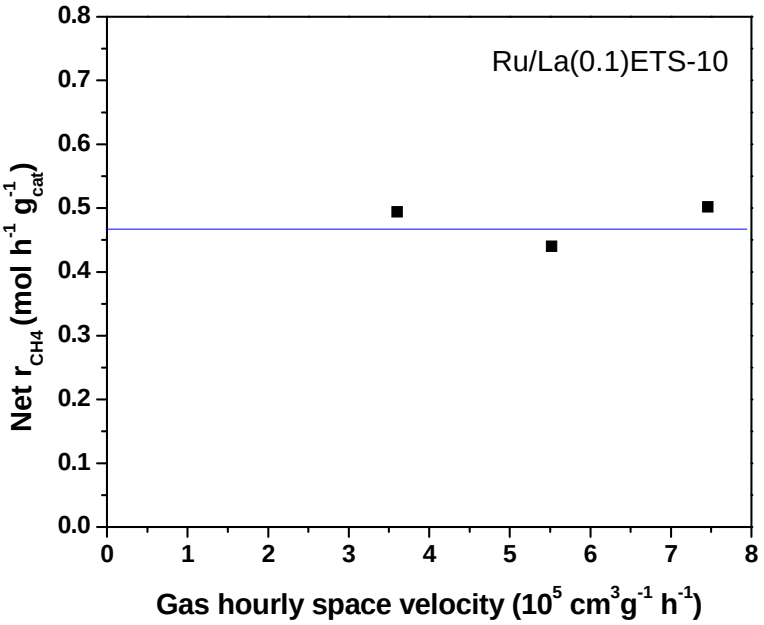
Ru/La(0.1)ETS-10
Net r_{CH4} (mol h^{-1} g_{cat}^{-1})
Gas hourly space velocity (10^5 $cm^3 g^{-1}$ h^{-1})
0.0
0.1
0.2
0.3
0.4
0.5
0.6
0.7
0.8
0
1
2
3
4
5
6
7
8